

Change of the Electronic Conductivity of CNTs and Graphene Sheets Caused by a Three-dimensional Strain Field

Masato Ohnishi

Department of Nanomechanics,
Graduate School of Engineering, Tohoku University
Sendai, Japan
masato.ohnishi@rift.mech.tohoku.ac.jp

Ken Suzuki, and Hideo Miura

Fracture and Reliability Research Institute,
Graduate School of Engineering, Tohoku University
Sendai, Japan
hmiura@rift.mech.tohoku.ac.jp

Abstract—The prediction of the change in the conductivity of carbon nanotubes (CNTs) and graphene nanoribbons (GNRs) under strain is very important to assure the reliability of the performance of CNT-based devices, such as transistors, sensors, actuators, etc. In this study, the change of the electronic state of CNTs and GNRs caused by their deformation was analyzed. We found that the change of the electronic state of CNTs was mainly dominated by two factors; (a) distortion of a six-membered ring due to the change in the C-C bond length and (b) increase in the local curvature of the tube. The increase of the curvature caused the orbital hybridization. The electronic state of GNRs also changed drastically when the hybridization was occurred by the curvature deformation.

Keywords—carbon nanotube; graphene nanoribbon; strain, conductivity, DFT, tight-binding approach

I. INTRODUCTION

Recently, physical and chemical properties of CNTs and graphene have been investigated by quite a few researchers all over the world in detail, and their unexpected superior characteristics have been made clear theoretically and experimentally. Many efforts to apply CNTs to various kinds of devices, such as transistors [1], biosensors [2], and mechanical strain sensors [3-4] have been made. Past studies have revealed that CNTs and graphene are prominent materials of devices of next generation. It is, however, difficult to realize the commercial use of CNTs or graphene sheets because of many difficulties. One of the biggest barriers to widespread commercial use of CNTs or graphene sheets is unexpected change of their electronic states caused by various internal and external factors; chirality (CNT), grain boundaries (graphene), defects, a magnetic fields, impurities, as well as external mechanical strain. For example, it is well known that the resistance of CNTs changes drastically under strain. Stampfer et al. showed large gauge factors (the ratio of change in the electrical resistance to the mechanical strain) in excess of 2900 [4]. Therefore, clarification of the effect of these factors on the electronic state of CNTs and graphene is important not only to assure the reliable performance of CNT- and graphene-based electronic devices but also to pave the way for the creation of revolutionary new devices.

In this study, we focused on the effect of the external mechanical strain on the electronic state of CNTs. In order to discuss the relationship between the deformation of a CNT and its electronic conductivity, the change of the geometric structure and the electronic state of CNTs under multi-axial strain was analyzed. Moreover, GNRs were used to analyze the effect of the hybridization in order to understand the effect of the hybridization in detail.

II. EFFECT OF THE DEFORMATION TO THE ELECTRONIC STATE OF CNTS

A. Deformation analysis of CNTs

In order to understand the deformation behavior of a CNT under strain, firstly deformation characteristics of CNTs under uni-axial strain were analyzed by using molecular dynamics (MD) simulation. The unit cell used in the deformation analysis consisted of a (17, 0) CNT with length 100.7 Å and the CNT was placed in the center of the cell. In the simulations, the periodic boundary condition is imposed on three dimensions. The basal surface area was enough large (> 100 Å × 100 Å) that the interaction between adjacent mirror cells could be neglected. The height of the cell was equal to the length of the CNT. All simulations were undertaken by using the Tersoff potential of LAMMPS package. NPT (300 K, 1 atm) simulations were firstly performed to acquire the equilibrium length of the CNT and obtained CNT length was defined as that in under stress (strain)-free condition. In the strain-free CNT structure, average bond length of C-C was 1.47 Å which is quite consistent with the experimental value [5]. Then, the height of the cell was changed with the velocity of 2.0 m/s to simulate the deformation of the CNT by uni-axial strain. In the deformation simulations, x and y coordinates of

TABLE I. Deformation analysis conditions.

Potential Function	Relaxation analysis		Loading analysis	
	Tersoff	NPT	Tersoff	Volume change
Ensemble	300 K	1.0 fs	300 K	1.0 fs
Temperature	10 ⁴	—	10 ⁶	—
Time Step	—	—	—	2.0 m/s
Total Step	—	—	—	—
Deformation Velocity	—	—	—	—

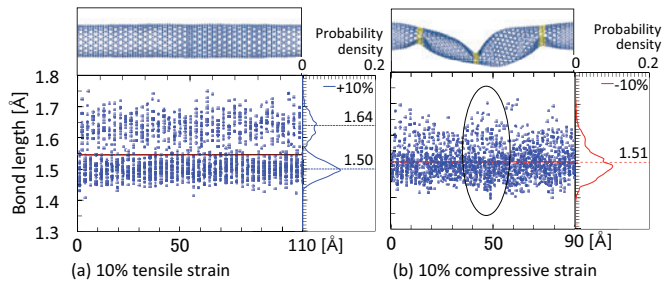


Figure 1. Change in distribution and probability distribution of C-C bond lengths and outlooks of a (17, 0) CNT under uni-axial strain.

atoms of the CNT at regions of 3 Å from both ends of the unit cell were fixed. Analysis conditions were summarized in Table I.

Examples of the spatial and frequency distribution of C-C bond lengths in the CNT with 10 % tensile and compressive uni-axial strain are shown in Fig. 1. The snapshots of deformed CNT structures are also shown in this figure. Fig. 1 (a) shows that the C-C bond length was elongated and distribution was separated into two major parts when the tensile strain was applied. One was in the range of 1.50 ± 0.4 Å and the other was 1.64 ± 0.8 Å. The ratio of these average bond lengths was about 1.2 in this case. The zigzag CNTs like a (17, 0) CNT have two types of C-C bonds in terms of the bond direction, (A) C-C bonds not parallel to the tube axis and (B) those parallel to the axis. Therefore, the separation of the bond length distribution indicates that C-C bonds parallel to the tube axis were elongated larger than that not parallel to the axis. As a result, six-membered rings in a CNT were distorted anisotropically under uni-axial tensile strain.

In the case of the axial compressive strain, the CNT showed simple shrinkage deformation when the amplitude of the applied compressive strain was less than 3%, and then the average bond length decreased monotonically (not shown here). The average bond length, however, increased when the amplitude of the applied compressive strain exceeded 3% (after buckling as shown in Fig. 1(b)). Fig. 1 (b) shows that the behavior of bond length change around buckling areas is different from that of other areas. Around the buckled area, the range of the distribution of C-C bond length was much larger than that obtained from other areas. Thus, buckling deformation of CNTs causes a very complicated strain distribution in the tube. Therefore, the clarification of the change mechanism of the electronic state of CNTs is very important to develop CNT-based devices.

B. Effect of the uni-axial strain to the electronic state of CNTs

From the deformation analysis using MD simulation, it was found that the ratio of the bond length in a six-membered carbon ring changes significantly when the uniaxial tensile strain is applied. In addition, the buckling deformation caused by uniaxial compressive strain introduces both axial and radial strain, and then enhances the anisotropic deformation of the six-membered ring locally. In this section, the effect of the distortion of a six-membered ring on the local electronic state of a CNT is analyzed in order to estimate the local conductivity

change caused by the application of tensile or compressive strain, respectively.

First, the change of the band gap of CNTs under uni-axial strain was calculated by using π orbital tight-binding approximation [6]. The hopping integral, which decreased exponentially with the increase in the bond length, was applied to this analysis [7]. Fig. 2 shows examples of the band gap change of a zigzag single-walled $(3n+p, 0)$ CNT ($n = 3, p = 0, \pm 1$) under uniform uni-axial strain from -10% to +20%. The amplitude of the applied uniaxial strain and the ratio of b/a , where a is the bond length not parallel to the axis and b is the bond length parallel to the axis as shown in Fig. 3(a), are shown in the minor and major axis, respectively. When the six-membered ring is without strain, the bond length ratio b/a is 1. When the absolute value of $(b/a - 1)$ becomes large, the six-membered ring is distorted heavily. In the case of $p = 0$ (metallic (9, 0) CNT), the band gap increased as the increase in both initial tensile and compressive strain (b/a ratio range from 0.93 to 1.12). On the other hand, in the case of $p = -1$ (+1) (semiconducting CNTs), the band gap decreased (increased) as the increase in a tensile strain while it increased (decreased) as the increase in a compressive strain when strain is small. These change behaviors were the same as all of $(3n+p, 0)$ zigzag CNTs ($n = 2, 3, 4, \dots, p = 0, \pm 1$).

The mechanism of the change in band gap can be understood by using Fig. 3(b-d). (9, 0) CNT was taken as an example. These figures show energy dispersions of graphene with uniaxial strain and solid lines in the figures indicate allowed wave vectors of the CNT, called cutting lines (CLs). The reciprocal spaces in these figures were depicted as the Brillouin zone and CLs remain invariant [6]. Since the energy dispersion of CNT can be obtained to trace that of graphene on

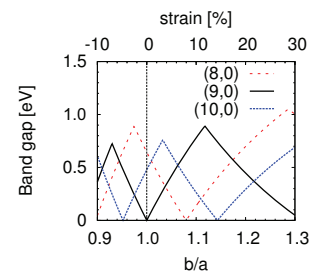


Figure 2. Effect of the ratio change of the C-C bond length (b/a) on the band gap of $(n, 0)$ CNT ($n = 8, 9, 10$).

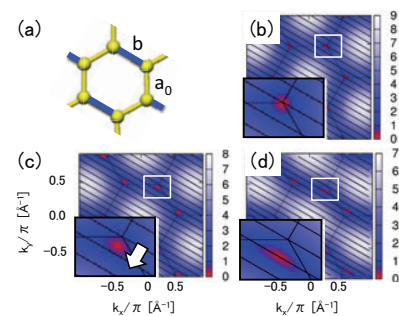


Figure 3. (a) Shape of a six-membered ring of a strained CNT and (b-d) a shift of the Fermi points of graphene and CLs of (9, 0) CNT. (b), (c), and (d) correspond to $b/a = 0.00, 1.12,$ and 1.30 , respectively.

CLs, the change behavior of the band gap of CNT can be understood as the shift of the Fermi points in the reciprocal space relative to CLs. At the unstrained state, the band gap was zero because the Fermi points were on CLs as shown in Fig. 3(b). The Fermi points, however, shifted perpendicular to the CLs when uni-axial strain was applied to the CNT, thus the band gap increased as the Fermi points receded from CLs. The value of band gap became maximum when the Fermi points were at the middle of two CLs as shown in Fig. 3(c), which corresponds to $b/a = 1.12$. When a further strain was applied to the CNT, the Fermi points approached to a next CL and, eventually, the band gap diminished when the Fermi points reached on CLs as shown in Fig. 3(d), which corresponds to $b/a \approx 1.30$. We concluded that the change in the bond length ratio caused the change in the band gap of the CNT. Therefore, such sensitivity of the band gap to the axial strain should cause the crucial change of conductivity of a deformed CNT.

C. Effect of the change in radial strain on the electronic state of CNTs

As was explained above, the ratio of the bond length in a six-membered carbon ring changes significantly when the uni-axial tensile strain is applied. In addition, the buckling deformation introduces strong radial strain to the tube. Thus, it is important to explicate the effect of the outer plane deformation of a six-membered ring on its electronic band structure. In this section, density functional theory (DFT) was applied to the analysis of the effect of outer plane deformation of a CNT on its electronic band structure.

It is estimated that the orbital hybridization, which changes the electronic state of CNT complicatedly, may occur between the π -orbital and σ -orbital of the six-membered carbon ring under the outer plane deformation. However, it is difficult to analyze the orbital hybridization by using the tight-binding approximation used in the former part of this section because it takes only the transfer integral and the overlap integral into account. Thus, the change of the electronic band structure of the deformed CNTs were analyzed by using Accelrys' DFT-code DMol³. The generalized gradient approximation (GGA) of PW91 was applied in this analysis. The total energy was converged to within 0.5 meV with a Monkhorst-Pack k -point mesh of $1 \times 1 \times 50$. The longitudinal direction of the CNTs was taken that along c axis and vacuum separations along both a and b axes were more than 50 Å, which was large enough to neglect the interaction of next cells. The length along c axis was equal to the transverse vector of CNTs.

In order to investigate the effect of outer plane deformation of a CNT on its electronic band structure, the radial strain is applied to a CNT. The change of the electronic states of (9, 0) CNTs, which had a radius of 3.5 Å corresponding to a curvature of 0.28 Å in the unstrained state, was used for the analysis. An axial and a radial strain were applied to the CNTs and the change of their electronic states was analyzed. During the radial strain loading, the shape of the cross section of a CNT was maintained as an ellipse and the bond lengths were fixed in this study. The semi-major axis of the ellipse was taken as $R = (1 - \epsilon_R)R_0$, where ϵ_R was defined the radial strain and R_0 was the radius of the unstrained CNT, 3.5 Å. The

amplitudes of the axial and the radial strains were varied from -5% to 20% and from 0% to 30%, respectively.

Fig. 4 summarizes the synergistic effects of axial and radial strain on the band gap of the CNT. Fig. 4(a) and (b) show the axial strain dependence of the band gap of the CNT with radial strain and radial strain dependence of the CNT with axial strain, respectively. Fig. 4(a) shows that a metallic (semiconducting) CNT changed to a semiconducting (metallic) CNT when axial strain was applied to the CNT with radial strain. However, the change in the band gap of the CNT with 30% radial strain was small when tensile strain was applied. In terms of the radial strain dependence, the band gap decreased monotonically with the increase of the radial strain as shown in Fig. 4(b). Even under the tensile strain, the CNT recovered from semiconducting characteristic to metallic characteristic when the radial strain was about 30%. Fig. 5 shows the change of the distribution of HOMO (highest occupied molecular orbital) and LUMO (lowest unoccupied molecular orbital) by 30% radial strain. The distribution of HOMO in the CNT with 30% radial strain shows that the orbital hybridization occurred around the region with large curvature. Therefore, the decrease of the band gap with increase of radial strain is due to the orbital hybridization between the π -orbital and σ -orbital. These results indicate that the electronic band structure, and thus, the electronic conductivity of the CNT varies drastically and complicatedly depending on the three-dimensional strain field. The amplitude of the change in the band gap of a CNT is a strong function of both the radial and axial strain.

III. Effect of orbital hybridization on the electronic state of GNRs

The application of radial strain on a CNT causes the generation of orbital hybridization which changes the magnitude of band gap of a CNT seriously. Therefore, in order to understand the effect of the orbital hybridization in a CNT in detail, we analyzed the change in the electronic state of GNRs. Electronic states of GNR under a longitudinal strain and

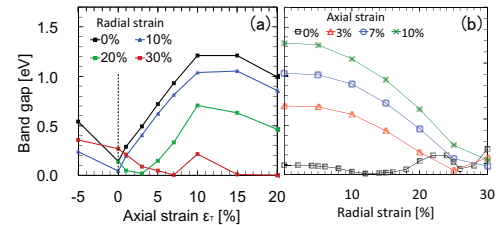


Figure 4. Effect of axial and radial strain on the band gap of a (9, 0) CNT. The results of Figs. (a) and (b) are same, while the axis strain and radial strain are taken as the transverse axes, respectively.

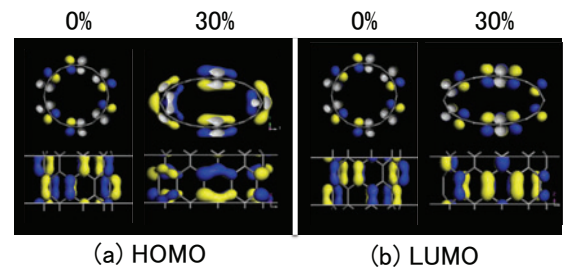


Figure 5. Change in (a) HOMO and (b) LUMO caused by applied radial strain. Axial strain was fixed at 0%.

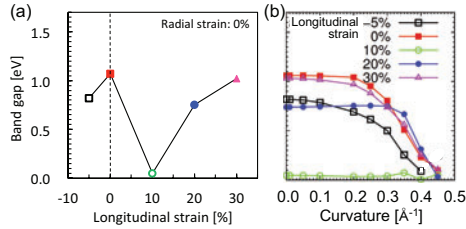


Figure 6. Change of the band gap of AGNR(N=10) caused by applied strain. (a) Effect of axial strain and (b) applied curvature are shown.

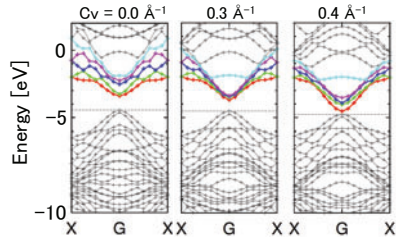


Figure 7. Change of electronic band structure of AGNR (N=10) caused by applied curvature (longitudinal strain: 0%)

applied curvature were analyzed. In this analysis, an armchair under multi-axial strain. Analysis method in this section is the same as that in section II-C. GNR (AGNR) with width of $N=10$, unzipped (5, 0) CNT, was used. All the dangling bonds of the GNR were terminated by hydrogen atoms. In addition, the nearest-neighbor bond length was fixed at the initial value during the application of a curvature. The radius of the initial (5, 0) CNT was 1.96 \AA , which corresponds to a curvature of 0.51 \AA^{-1} . The amplitude of the applied longitudinal strain and that of the curvature were varied from -5% to 30% and from 0.00 to 0.45 \AA^{-1} , respectively. The electronic properties of the AGNR ($N=10$), which has a band gap of 1.1 eV in the unstrained state, changed to metallic state when the longitudinal tensile strain of 10 % was applied as shown Fig. 6(a). This semiconducting-metal transition by longitudinal strain is the same feature as that of CNTs by axial strain. When the curvature was applied to the semiconducting AGNR, the band gap of the AGNR started to decrease drastically when the applied curvature exceeded about 0.3 \AA^{-1} , regardless of the amplitude of the applied longitudinal strain as shown Fig. 6(b). Fig. 7 shows an example of the change of the electronic band structure of the AGNR under the applied curvature. In this example, the longitudinal strain was fixed at 0 %. When the amplitude of the applied curvature was less than 0.3 \AA^{-1} , the third and fourth excitation energies (blue and pink) decreased with the increase of curvature, though dispersions of the first and the second excitation energies (red and green) did not change significantly. Once the curvature reached 0.3 \AA^{-1} , orbital hybridization started to occur, and the first and the second excitation energies decreased drastically. This result indicates that the first and the second band energies, which are dominant on the electronic conductivity, do not change significantly when the amplitude of the applied curvature is small. They, however, decrease drastically once hybridization occurred, and it causes the decrease of band gap of the GNR. This result suggests the existence of threshold value of curvature or radial strain of a CNT introducing orbital hybridization. Therefore, it is very important to control the shape of a CNT for assuring the reliable performance of CNT-

based electronic devices because the electronic state of a CNT is very sensitive to not only axial strain but also radial strain (curvature of the tube).

IV. CONCLUSION

In this study, the change of the configuration structure and the electronic state of CNTs and GNRs caused by deformation was analyzed by applying a molecular dynamics, a tight-binding approach and the DFT calculation. Since the conductivity change is caused by the deformation of the CNT, deformation characteristics of CNTs under axial strain were investigated. We found that six-membered rings in a CNT were distorted under both uni-axial tensile and compressive strain significantly. Especially, buckling deformation of CNTs causes the change of the very complicated strain distribution and the increase in the local curvature in a tube. To understand the effect of the uniform uni-axial strain, the band gap change of CNTs under uni-axial strain was calculated by using a tight-binding approach. The bond length ratio b/a was found to be a dominant factor that changes the electronic state of CNTs under strain. Since the buckling deformation introduced a local radial strain and thus orbital hybridization in a CNT, the change of the electronic state of both CNTs and GNRs, under radial strain and applied curvature, respectively, was analyzed by using the DFT. We clarified that the electronic band structure of the deformed CNT varies drastically and complicatedly depending on the three-dimensional strain filled in it. Therefore, the electronic conductivity of a GNR and thus, a CNT was found to be mainly dominated by the fluctuation of the distance between the nearest carbons.

ACKNOWLEDGMENT

This research was partly supported by the Grants-in-Aid for Scientific Research and the Japanese special coordination funds for promoting science and technology.

REFERENCES

- [1] A. Bachtold, P. Hadley, T. Nakahishi, and C. Dekker, "Logic circuits with carbon nanotube transistors," *Science* 294, 1317 (2001).
- [2] A. Star, J. C. P. Gabriel, K. Bradley, and G. Grüner, "Electronic detection of specific protein binding using nanotube FET devices," *Nano Lett.*, Vol. 3, No. 4, 459-463 (2003).
- [3] M. Ohnishi, K. Ohsaki, Y. Suzuki, K. Suzuki, and H. Miura, "Nanostructure dependence of the electronic conductivity of carbon nanotubes and graphene sheets," *Proc. of the ASME 2010 International Mechanical Engineering Congress & Exposition, IMECE2010-37277*, 1-7 (2010).
- [4] C. Stampfer, A. Jungen, R. Linderman, D. Oberfell, S. Roth, and C. Hierold, "Nano-electromechanical displacement sensing based on single-walled carbon nanotube," *Nano Lett.* Vol. 6, No. 7, pp. 1449-1453 (2006).
- [5] T. W. Odom, J. L. Huang, P. Kim, and C. M. Lieber, "Atomic structure and electronic properties of single-walled carbon nanotubes," *Nature*, 391, 62 (1998).
- [6] L. Yang, and J. Han, "Electronic structure of deformed carbon nanotubes," *Phys. Rev. Lett.* 85, 1, 154-157 (2000).
- [7] V. M. Pereira, A. H. C. Neto, and N. M. R. Peres, "Tight-binding approach to uniaxial strain in graphene," *Phys. Rev. B* 80, 045401 (2009).
- [8] J. Q. Lu, J. Wu, W. Duan, F. Liu, B. F. Zhu, and B. L. Gu, "Metal-to-Semiconductor Transition in Squashed Armchair Carbon Nanotubes," *Phys. Rev. Lett.* 18, 15, 156601-1, 2003.